REPORT

Regulation of Golgi turnover by CALCOCO1-mediated selective autophagy

Thaddaeus Mutugi Nthiga, Birendra Kumar Shrestha, Jack-Ansgar Bruun, Kenneth Bowitz Larsen, Trond Lamark, and Terje Johansen

The Golgi complex is essential for the processing, sorting, and trafficking of newly synthesized proteins and lipids. Golgi turnover is regulated to meet different cellular physiological demands. The role of autophagy in the turnover of Golgi, however, has not been clarified. Here we show that CALCOCO1 binds the Golgi-resident palmitoyltransferase ZDHHC17 to facilitate Golgi degradation by autophagy during starvation. Depletion of CALCOCO1 in cells causes expansion of the Golgi and accumulation of its structural and membrane proteins. ZDHHC17 itself is degraded by autophagy together with other Golgi membrane proteins such as TMEM165. Taken together, our data suggest a model in which CALCOCO1 mediates selective Golgiphagy to control Golgi size and morphology in eukaryotic cells via its interaction with ZDHHC17.

Introduction

Degradation of protein aggregates, invading pathogens, and damaged organelles by macroautophagy (henceforth autophagy) is important for maintaining eukaryotic cell function, health, and survival. Autophagy is an evolutionarily conserved process in which cytoplasmic material is sequestered into double-membraned vesicles called autophagosomes, which then fuse with lysosomes to degrade their contents. At the basal level, autophagy facilitates constitutive turnover of cytoplasmic contents to maintain cellular homeostasis. During nutrient starvation, autophagy degrades macromolecules such as lipids, carbohydrates, and proteins to recycle nutrients and generate energy (Ohsumi, 2014; Dikic and Elazar, 2018; Feng et al., 2014).

Evolutionarily conserved autophagy-related proteins (ATGs), acting in temporal hierarchical complexes, regulate the formation and expansion of phagophores to form autophagosomes. Autophagosome formation is initiated and nucleated at ER membranes by the ULK and PI3KC3 complexes. Their coordinated action at the phagophore formation site generates phosphatidyl-inositol-3-phosphate, which in turn recruits lipid-binding proteins WIPI (WD repeat domain, phosphoinositide-interacting protein) and DFCP1. Phagophore expansion is initiated by WIPI-dependent recruitment of ATG2 and ATG12-ATG5:ATG16L1 complex. The latter, acting as an E3 ligase with the E1 enzyme ATG7 and E2 enzyme ATG3, facilitates lipidation of ATG8 proteins on the phagophore (Ohsumi, 2014; Zaffagnini and Martens, 2016; Kirkin and Rogov, 2019). The ATG2–WIPI complex transfers lipids to the phagophore, as does also ATG9, the only transmembrane core autophagy protein (Maeda et al., 2019; Maeda et al., 2020; Matoba

et al., 2020; Osawa et al., 2019; Valverde et al., 2019). ATG9 vesicles also contribute directly to phagophore formation (Dikic and Elazar, 2018; Yu et al., 2018). Lipidated ATG8s act as scaffolds for recruitment of cargos and essential autophagy proteins for phagophore growth and closure (Lystad and Simonsen, 2019; Johansen and Lamark, 2020).

Autophagy acts selectively in the degradation of organelles, protein aggregates, or invading foreign agents (Johansen and Lamark, 2011). The selectivity is mediated by receptor proteins, which link degradable cargo to phagophore membranes by binding to LC3/GABARAP proteins on the phagophore membrane via LC3-interacting region (LIR) and/or Ubiquitin-like interacting motif (Birgisdottir et al., 2013; Johansen and Lamark, 2020; Marshall et al., 2019; Pankiv et al., 2007; Rogov et al., 2014). The cell engages selective autophagy as a form of organelle autoregulation to control the capacity, number, and integrity of organelles in accordance with cellular demands. Surplus or damaged organelles or portions of organelles are selectively cleared to counter stress response mechanisms, which typically increase the number or volume of organelles to alleviate the vagaries of cellular stress. For instance, the unfolded protein response increases ER volume and expression of ER-resident proteins to augment the capacity of the ER to alleviate stress. Subsequently, ER-phagy is engaged to selectively degrade excess ER to restore homeostasis (Wilkinson, 2019; Hübner and Dikic, 2020).

Selective autophagy of cellular organelles is mediated by specific autophagy receptors (Johansen and Lamark, 2020;

Molecular Cancer Research Group, Department of Medical Biology, University of Tromsø – The Arctic University of Norway, Tromsø, Norway.

Correspondence to Terje Johansen: terje.johansen@uit.no; Trond Lamark: trond.lamark@uit.no.

Kirkin and Rogov, 2019). The Golgi apparatus, however, has not been associated with any known autophagy degradation mechanism or selective autophagy receptors. The Golgi processes and sorts secretory and membrane proteins by adding modifications such as glycosylation and sulfation, before the proteins are sent to their destinations by vesicular transport (Farquhar, 1985). The Golgi stress response is less studied than the ER stress response, but involves increased synthesis of Golgi structural proteins, glycosylation enzymes, and vesicular transport components (Oku et al., 2011). It is tempting to speculate that yet-to-be-identified autophagy mechanisms are involved in degradation of the Golgi.

Several selective autophagy receptors mediate degradation of the same type of organelles. In ER-phagy, six different receptors have been identified so far (Wilkinson, 2019). We also recently identified CALCOCO1 as an ER-phagy receptor (Nthiga et al., 2020). CALCOCO1 mediates ER-phagy by interacting with VAMP-associated protein (VAP) on the ER membrane via a two phenylalanines (FF) in an acidic tract (FFAT)–like motif and with LC3/GABARAP proteins via LIR and UDS-interacting region (UIR) motifs. A fraction of CALCOCO1 is localized to the Golgi, suggesting a Golgi-related function. In this study, we identified CALCOCO1 as a receptor for autophagic degradation of Golgi during starvation. This requires CALCOCO1 binding to the ankyrin repeat (AR) domain of ZDHHC17 and ZDHHC13 via a ZDHHC-AR–binding motif (zDABM). ZDHHC17 and -13 are Golgi-localized transmembrane S-acyltransferases (also called palmitoyltransferases; Ernst et al., 2018). Depletion of CALCOCO1 causes an expansion of the Golgi and accumulation of Golgi-resident proteins. CALCOCO1 mediates Golgiphagy to regulate Golgi remodeling during stress.

Results and discussion

Interaction of CALCOCO1 with ZDHHC17 via a zDABM motif
We identified Golgi-localized ZDHHC17 and ZDHHC13 S-acyltransferases in an affinity purification mass spectrometry–based screen for CALCOCO1 interactors (Fig. 1 A; Nthiga et al., 2020). S-acyltransferases catalyze protein S-acylation reactions (also called palmitoylation), a reversible addition of fatty acids, usually palmitate, to cysteines of proteins. Palmitoylation plays a major role in regulating membrane targeting, trafficking, stability, and function of the modified proteins (Fukata and Fukata, 2010; Linder and Deschenes, 2007). Of the 24 palmitoyltransferases in mammals, only ZDHHC17 and ZDHHC13 contain an N-terminal AR domain. Both ZDHHC17 and ZDHHC13 are localized in the Golgi (Ernst et al., 2018), but a separate study reported localization of ZDHHC13 also to the ER (Ohno et al., 2006). In humans, ZDHHC17 is highly expressed in the brain, and knockout (KO) in mice significantly affected synaptic plasticity and produced Huntington-like symptoms (Ohno et al., 2006; Sanders et al., 2015). The AR domains of ZDHHC17 and -13 function in both substrate recruitment and S-acylation–independent functions (Lemonidis et al., 2017; Verardi et al., 2017). The AR domain interacts with proteins bearing zDABM (Lemonidis et al., 2015).

We recently reported that CALCOCO1 is localized in the Golgi (Nthiga et al., 2020). To investigate whether CALCOCO1

interacts and colocalizes with ZDHHC17 and -13 on the Golgi, we co-expressed EGFP-CALCOCO1 and Myc-ZDHHC17 in CALCOCO1 KO HeLa cells. A significant fraction of EGFP-CALCOCO1 colocalized completely with ZDHHC17 and cis-Golgi protein GM130 (Fig. 1, B and C). Similarly, EGFP-CALCOCO1 colocalized with Myc-ZDHHC13 on the Golgi (Fig. S1 A), suggesting that CALCOCO1 and ZDHHC17 and -13 interact in cells and colocalize in the Golgi. GST-ZDHHC17 pulled down in vitro-translated Myc-CALCOCO1 in a GST pull-down assay (Fig. 1 D), suggesting a direct interaction of CALCOCO1 with ZDHHC17.

The critical residues in the AR domain of ZDHHC17 for binding to the zDABM motif are N100/W130 (Verardi et al., 2017). We tested the effect of point mutations of these residues on ZDHHC17 binding to CALCOCO1. Alanine substitutions (N100A/W130A) abolished the interaction of ZDHHC17 with CALCOCO1 (Fig. 1 D), indicating that the interaction is mediated by the AR–zDABM interface. The zDABM motif has a (VIAP) (-VIT)XXQP core consensus sequence, where X is any amino acid (Lemonidis et al., 2015). CALCOCO1 has a similar motif encompassing 574-VVISQP-579 in the C-terminal half of the protein. Mutation of the critical binding residues within this motif (Lemonidis et al., 2017) to alanines (574-AAISAA-579) abolished the interaction of CALCOCO1 with ZDHHC17 (Fig. 1 D), suggesting that the 574-VVISQP-579 sequence is a zDABM motif (Fig. 1 E). CALCOCO1 self-oligomerizes via its coiled-coil domain. Deletion of the coiled-coil domain did not affect the interaction with ZDHHC17 (Fig. 1 F), implying that CALCOCO1 self-oligomerization has no effect on the binding of its zDABM motif to ZDHHC17.

CALCOCO1 is a paralog to TAX1BP1 and NDP52. These three selective autophagy receptors share substantial sequence similarity and identity. While no potential zDABM motif was identified in NDP52, we identified a potential motif in TAX1BP1 encompassing 673-VVCSQP-678. While WT ZDHHC17 interacted with TAX1BP1 in GST pull-down assays, the interaction was abolished by the N100A/W130A mutations (Fig. 1 G), indicating that the ZDHHC17 interaction with TAX1BP1 was mediated by the AR–zDABM interface. Conversely, when the VVCSQP sequence in TAX1BP1 was deleted, the interaction with ZDHHC17 was completely abrogated (Fig. 1 G), indicating that the 673-VVCSQP-678 sequence in TAX1BP1 is a zDABM motif. Hence, CALCOCO1 and TAX1BP1 share a similar mechanism of interaction with ZDHHC17 and -13. While fractions of both EGFP-CALCOCO1 and EGFP-CALCOCO1-mutzDABM colocalized with Myc-ZDHHC17 on the Golgi, EGFP-CALCOCO1-mutzDABM colocalized significantly less with Myc-ZDHHC17 than EGFP-CALCOCO1 (Fig. S1, A–C). Thus, the interaction of CALCOCO1 with ZDHHC17 is important for recruitment of CALCOCO1 to the Golgi.

CALCOCO1 recruits starvation-induced Golgi fragments to autophagosomes
Golgi is fragmented in stress conditions such as viral infection and nutrient starvation (Campadelli et al., 1993; Takahashi et al., 2011). Upon starvation, Golgi fragments disperse in the cytoplasm and colocalize with autophagosomes (Takahashi et al., 2011). Because CALCOCO1 is localized on the Golgi and binds
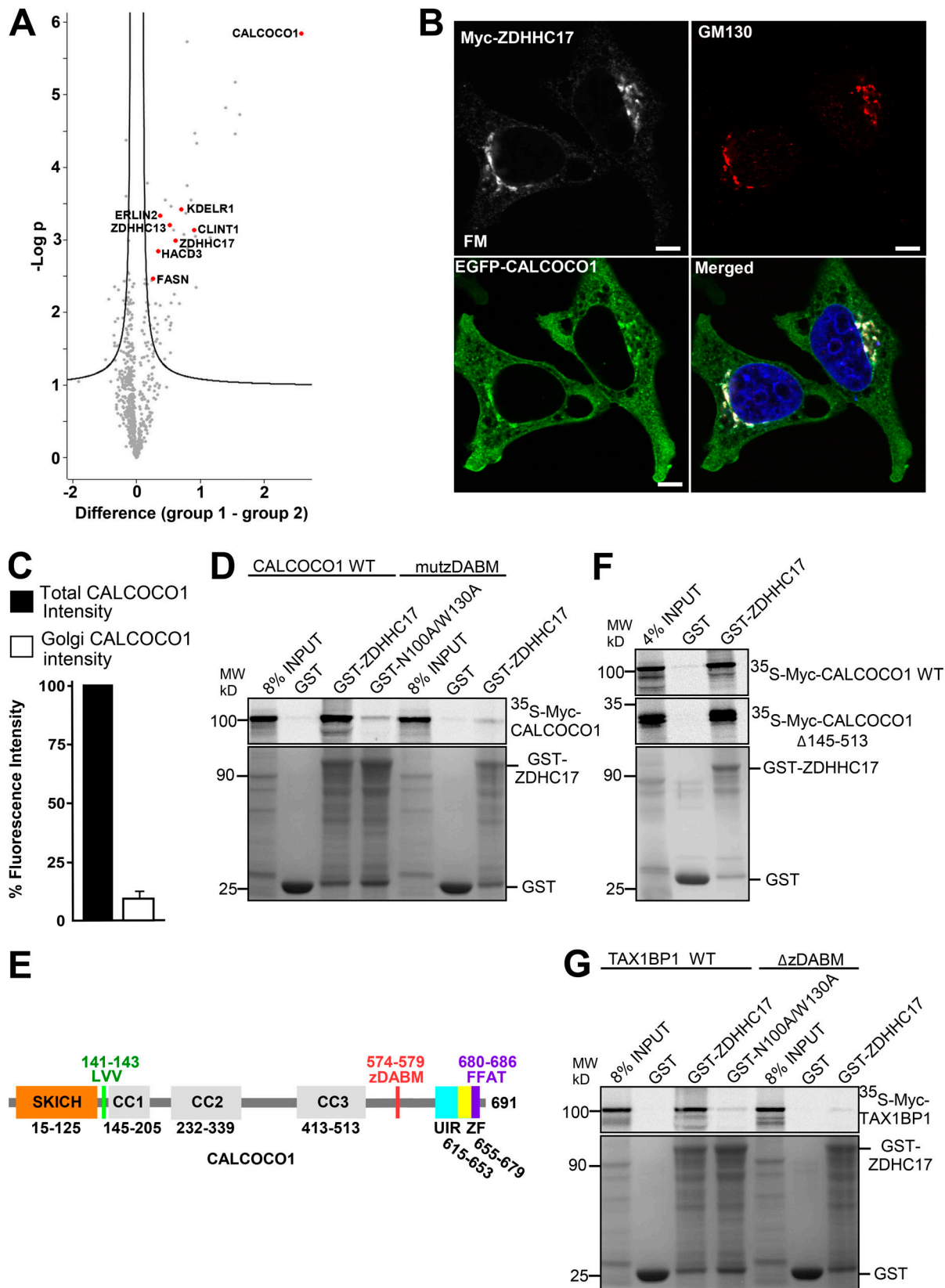
Figure 1. **CALCOCO1 interacts with ZDHHC17 via zDABM motif. (A)** Volcano plot showing some of the Golgi- and ER-localized proteins that were identified in the CALCOCO1-interactome screen. Three independent immunoprecipitations and MS analyses were conducted with EGFP-CALCOCO1 as bait. Only some of the identified proteins are shown. **(B)** HeLa CALCOCO1 KO cells were transiently cotransfected with Myc-ZDHHC17 and EGFP-CALCOCO1 cultured in full medium and immunostained with anti-GM130 antibody. We used CALCCO1 KO cells to avoid interference by endogenous CALCOCO1. Scale bars represent 5 μm. **(C)** Fluorescence intensity analysis of EGFP-CALCOCO1 in the cells analyzed in B. The error bars represent mean ± SD of three independent experiments

with 100 cells per experiment. **(D)** GST, GST-ZDHHC17, or GST-ZDHHC17(N100A/W130A) was used in pull-down against in vitro translated Myc-CALCOCO1 or Myc-CALCOCO1-mutzDABM (mutant zDABM). **(E)** Domain architecture of human CALCOCO1 showing the location of zDABM motif relative to other domains. **(F)** GST or GST-ZDHHC17 was used in pull-down against in vitro translated Myc-CALCOCO1 or Myc-CALCOCO1 Δ145–513. **(G)** GST, GST-ZDHHC17, or GST-ZDHHC17(N100A/W130A) was used in pull-down against in vitro translated Myc-TAX1BP1 or Myc-TAX1BP1-ΔzDABM (ΔzDABM, zDABM deleted). MW, molecular weight.

---

both ZDHHC17 and LC3/GABARAP proteins (Nthiga et al., 2020), we asked if starvation-induced Golgi fragments would colocalize with CALCOCO1 in the cytoplasm and autophagosomes. Thus, we transiently co-expressed Myc-ZDHHC17 with EGFP-CALCOCO1 in CALCOCO1 KO HeLa cells and monitored the Golgi morphology under normal and starvation conditions in the presence of bafilomycin A1 (BafA1). We used BafA1 to inhibit lysosomal degradation of LC3B-positive Golgi fragments and vesicles. The colocalization of EGFP-ZDHHC17 with endogenous TMEM65 on the Golgi indicated that the overexpressed EGFP-ZDHHC17 was not mislocalized (Fig. 2 A). Under normal culture conditions, the Golgi, as visualized with EGFP-ZDHHC17 and endogenous TMEM165, formed intact stacks with ribbon-like morphology (Fig. 2, A and B) that colocalized with a fraction of the EGFP-CALCOCO1 but not with autophagosome marker LC3B (Fig. 2 B). Upon nutrient starvation, Myc-ZDHHC17 and TMEM165 lost the characteristic ribbon-like morphology of the Golgi and formed fragmented and dispersed vesicular structures (Fig. 2, A–C). Fragmentation also occurred in CALCOCO1 KO cells (Fig. 2 C), suggesting that CALCOCO1 is not required for Golgi fragmentation during starvation. The ZDHHC17-positive Golgi fragments colocalized both with EGFP-CALCOCO1 and with endogenous LC3-positive vesicles (Fig. 2, B and D). This shows recruitment of the fragments to autophagosomes, consistent with a recent report of sequestration of Golgi fragments into autophagosomes during starvation (Lu et al., 2020). The colocalization with LC3B-positive vesicles was reduced in CALCOCO1 KO cells (Figs. 2 D and S1 D), indicating that CALCOCO1 mediated recruitment of a fraction of Golgi fragments to autophagosomes. To clarify if the recruitment was via CALCOCO1 interacting with LC3/GABARAP proteins during starvation, EGFP-CALCOCO1 was expressed and immunoprecipitated from starved and BafA1-treated HeLa cell extracts. Co-precipitation of endogenous LC3B-II indicated efficient interaction of CALCOCO1 with LC3B-II during starvation (Fig. 2 E). Hence, CALCOCO1 recruits a fraction of starvation-induced Golgi fragments to autophagosomes via interaction with LC3/GABARAP proteins.

ZDHHC17 promotes Golgiphagy during starvation

The highly dynamic Golgi apparatus is regulated by physiological demands and likely by a stress response akin to the regulation of the ER by the ER stress response. The Golgi stress response augments the capacity of the Golgi by increasing synthesis of structural Golgi proteins such as GM130, GCP60, and giantin; glycosyltransferases; and vesicular transport components (Sasaki and Yoshida, 2015; Oku et al., 2011). It is not known if autophagy is involved in turnover of excess Golgi membranes to remodel the Golgi back to physiological size. We postulated that the Golgi is remodeled back to physiological size by autophagy-mediated degradation of the excess membranes and

proteins produced by the stress response. By monitoring the turnover of Golgi structural and membrane proteins during nutrient starvation, we found that in WT murine embryo fibroblast (MEF) cells, levels of Golgi structural protein GM130 and Golgi membrane proteins TMEM165 and ZDHHC13 were significantly reduced after 6 h of starvation. The decrease was blocked by BafA1 (Fig. 3, A and B), suggesting autophagy-mediated degradation. Consistently, in ATG5 KO MEFs, the starvation-induced turnover of the proteins was impaired compared with WT MEFs (Fig. 3, A and B). Also, starved ATG5 KO MEFs had higher levels of these proteins than starved WT MEFs. Similarly, starved ATG7 KO HeLa cells had increased amounts of GM130, TMEM165, and ZDHHC13 relative to WT HeLa cells (Fig. S2 A). Furthermore, HBSS + Baf A1–treated WT HeLa cells, and not ATG7 KO cells, had higher amounts of these proteins than cells treated with HBSS only (Fig. S2 A), indicating autophagic degradation. The accumulation of Golgi proteins in the two autophagy-deficient cell types during starvation and their accumulation in WT cells upon HBSS + Baf A1 treatment were similar to the accumulation of autophagy receptors p62 and CALCOCO1 in these cells (Fig. 3, A and B), suggesting that the Golgi proteins are also autophagy substrates. We conclude that autophagy is involved in degrading Golgi structural and membrane proteins during starvation.

ZDHHC17 and -13 are cis-Golgi integral membrane proteins. Their degradation by autophagy and interaction with CALCOCO1 made us ask if they mediated the observed degradation of the Golgi. Hence, we made HeLa cells with inducible expression of EGFP-ZDHHC17 and monitored the turnover of Golgi transmembrane protein TMEM165. Starvation induced a decrease in EGFP-ZDHHC17 and TMEM165 not seen in the noninduced cells that was blocked by BafA1 treatment (Fig. 3, C–E). Hence, ZDHHC17 is degraded by autophagy, and its overexpression promotes Golgiphagy during starvation. The amounts of the ER protein VAPA were similar in induced and noninduced cells (Fig. 3 C), suggesting that the ZDHHC17-mediated degradation was selective for the Golgi. Expression of EGFP-ZDHHC17 in HeLa CALCOCO1 KO cells reduced the level of TMEM165 in cells treated with HBSS (Fig. S2 B). Thus, elevated expression of ZDHHC17 may induce Golgiphagy also in cells lacking CALCOCO1, but the effect was less pronounced than in WT cells (Fig. 3 C), and TMEM165 was not stabilized by treatment with HBSS + BafA1 (Fig. S2 B). In WT cells, expression of the EGFP-ZDHHC17 N100A/W130A mutant did not reduce TMEM165 levels in cells treated with HBSS (Fig. S2 B). Thus, the zDABM motif is needed for Golgiphagy induced by elevated expression of ZDHHC17. Together, our data clearly suggest impaired autophagic Golgi degradation when CALCOCO1 is depleted or the CALCOCO1–ZDHHC17 interaction is compromised.
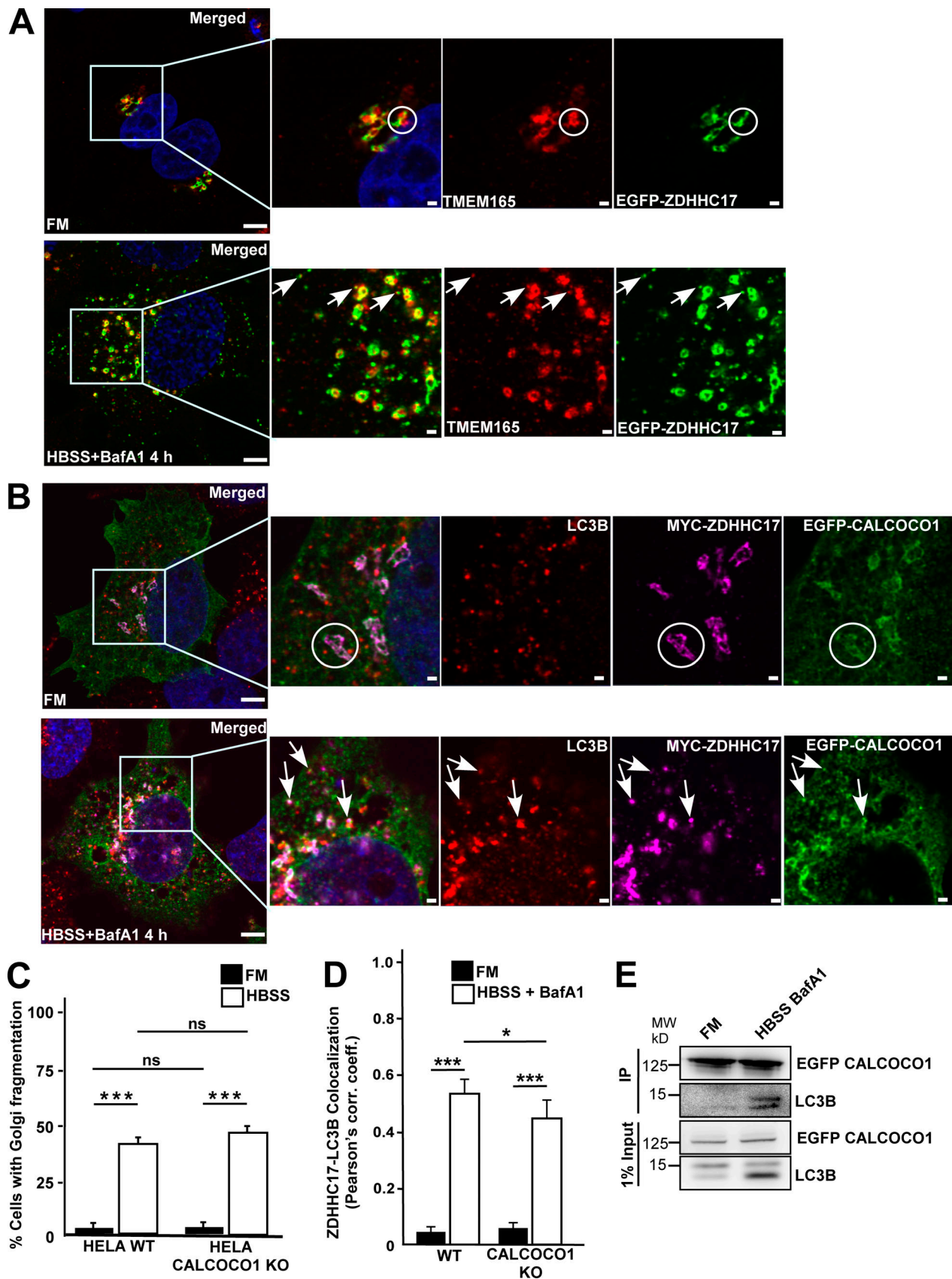
Figure 2. **CALCOCO1 recruits starvation-induced Golgi fragments to autophagosomes. (A)** HeLa WT cells were transfected with EGFP-ZDHHC17; 24 h after transfection, they were either left untreated or starved (HBSS) for 4 h with Baf A1 treatment, then stained for endogenous TMEM165. Bars represent 5 µm (main) and 1 µm (insets). **(B)** HeLa WT cells were cotransfected with Myc-ZDHHC17 and EGFP-CALCOCO1; 24 h after transfection, they were either left

untreated or starved for 4 h with Baf A1 treatment and then immunostained for endogenous LC3B. The arrows in A and B point to colocalization. Bars represent 5 μm (main) and 1 μm (insets). **(C)** HeLa WT and HeLa-CALCOCO1 KO cells were transfected with EGFP-ZDHHC17; 24 h after transfection, they were either left untreated or starved for 6 h. The number of cells with fragmented Golgi phenotype was manually counted and weighted against the total number of cells. **(D)** Colocalization analysis of ZDHHC17 and LC3B in WT cells analyzed in B and CALCOCO1 KO cells analyzed in Fig. S1 D. The error bars in C and D represent mean ± SEM of three independent experiments per condition with 100 cells per experiment. Statistical comparison was analyzed by one-way ANOVA followed by Tukey multiple comparison test. Significance is displayed as ***, P < 0.001; * P < 0.01. corr. coeff., correlation coefficient. **(E)** EGFP-CALCOCO1 was transiently expressed in HeLa WT cells; 24 h after transfection, the cells were either left untreated or starved and treated with Baf A1. EGFP-CALCOCO1 was then immunoprecipitated (IP) from cell extracts using GFP-TRAP. EGFP-CALCOCO1 and coprecipitated endogenous LC3B were visualized by Western blotting using anti-GFP and anti-LC3B antibodies. MW, molecular weight.

We used immunofluorescence to assess delivery of ZDHHC17-containing autophagosomes to lysosomes in WT, CALCOCO1 KO, and autophagy-deficient ATG7 KO cells. To adequately capture autophagosome-lysosome colocalization, cells were treated with BafA1. In WT cells under basal conditions, EGFP-ZHHC17 formed intact stacks with ribbon-like morphology that did not colocalize with LC3B or lysosomal marker LAMP2 (Fig. 3, F and G). Upon starvation, EGFP-ZDHHC17 formed cytoplasmic puncta that colocalized with both LC3B and LAMP2 (Fig. 3, F and G), suggesting that ZDHHC17-containing autophagosomes are delivered to the lysosomes during starvation. In CALCOCO1 KO and ATG7 KO cells, the colocalization of EGFP-ZDHHC17 cytoplasmic puncta with LAMP2 during starvation was significantly reduced compared with WT cells (Figs. 3 G, S1 D, and S2 D). Hence, delivery of a significant fraction of the Golgi-derived ZDHHC17-containing vesicles to lysosomes is mediated by CALCOCO1 and is dependent on macroautophagy.

Depletion of CALCOCO1 decreases Golgiphagy
We applied mCherry-EYFP tandem tagging of ZDHHC17 and TMEM165 to monitor and compare the Golgi turnover in HeLa WT, CALCOCO1 KO, and ATG7 KO cells. EYFP is unstable, while mCherry is stable in the acidic environment of the lysosomes. Consequently, mCherry-EYFP–containing autolysosomes appear as red-only puncta (Pankiv et al., 2007). Cells with more autophagy flux have a higher red-only puncta/total puncta ratio. When transiently transfected mCherry-EYFP-ZDHHC17 and mCherry-EYFP-TMEM165 were monitored by confocal microscope under starvation conditions, the ratios of red-only (mCherry) puncta to total puncta were much higher in WT cells than in CALCOCO1 KO and ATG7 KO cells (Fig. 4, A–D; and Fig. S3 A), clearly showing that Golgiphagy is significantly decreased in the absence of CALCOCO1.

CALCOCO1 is a selective Golgiphagy receptor
To clarify the role of CALCOCO1 in the turnover of Golgi membrane components, we investigated how this turnover was affected by the presence or absence of CALCOCO1. During starvation, the amounts of the Golgi proteins GM130, TMEM165, and ZDHHC13 were clearly higher in CALCOCO1 KO cells than in WT cells (Fig. S3 B), suggesting impaired Golgi turnover. CALCOCO1 KO had no significant effect on starvation-induced degradation of autophagy receptor NDP52 (Fig. S3 B). To enable a more controlled investigation, we reconstituted CALCOCO1 KO cells with inducible EGFP-CALCOCO1 and monitored the effect on Golgi protein levels. In noninduced cells, HBSS strongly increased the amount of Golgi proteins ZDHHC13, GM130, and

TMEM165 (Fig. 5, A and B). In cells expressing EGFP-CALCOCO1, there was autophagic degradation of the proteins, as indicated by their higher amounts in cells treated with HBSS + BafA1 than in cells treated with HBSS only (Fig. 5, A and B). In the noninduced cells, the amounts of the proteins in both HBSS + BafA1– and HBSS-only–treated cells were equal (Fig. 5, A and B), suggesting impaired or reduced Golgiphagy in the absence of CALCOCO1. Interestingly, the amounts of the proteins in the uninduced MG132-treated cells were higher than in the similarly treated induced cells. Because MG132 treatment causes proteotoxic stress, the lower amounts of proteins in induced cells than in uninduced cells suggests that CALCOCO1 plays a role in degrading the Golgi during proteotoxic stress. In a similar experiment in CALCOCO1 KO cells reconstituted with inducible EGFP-CALCOCO1-mutzDABM, a mutant that is incapable of ZDHHC17 interaction, the amounts of TMEM165 in the HBSS-only–treated cells were comparatively equal in the induced and noninduced cells. HBSS + BafA1 treatment did not increase the amounts further (Fig. 5, C and D), suggesting reduced or impaired degradation by the lack of CALCOCO1–ZDHHC17 interaction. Together, these results suggest that CALCOCO1 mediates autophagic degradation of the Golgi components via interaction with ZDHHC17. Starvation-induced degradation of VAPA was not impaired by the zDABM mutation (Fig. 5, C and D), indicating that ER-phagy mediated by CALCOCO1 is independent of the ZDHHC17 interaction.

To corroborate our findings that CALCOCO1 mediated Golgiphagy, we monitored, by immunofluorescence, the labeling intensity of endogenous GM130 in CALCOCO1 KO cells in the presence or absence of induced or noninduced EGFP-CALCOCO1. When EGFP-CALCOCO1 was induced for 24 h under basal conditions, the average GM130 intensity was relatively lower in induced cells than in noninduced cells (Fig. 5 E), suggesting decreased amounts of the protein due to CALCOCO1 expression. The intensity in both the induced and noninduced cells increased when the cells were treated with BafA1 for 6 h before intensity measurement, suggesting degradation of GM130 by Golgiphagy. When the cells were starved for 2 h first, the average GM130 intensity was relatively lower in induced than in noninduced cells (Fig. 5 E), suggesting CALCOCO1-dependent turnover of GM130 during starvation.

To clarify if the observed turnover of Golgi components was mediated by CALCOCO1 interaction with ATG8 proteins, CALCOCO1 KO cells reconstituted with EGFP-CALCOCO1 mLIR + Δ623–691, a deletion mutant incapable of interacting with ATG8 proteins, were used to monitor turnover of Golgi structural and membrane proteins. Induced expression of EGFP-CALCOCO1
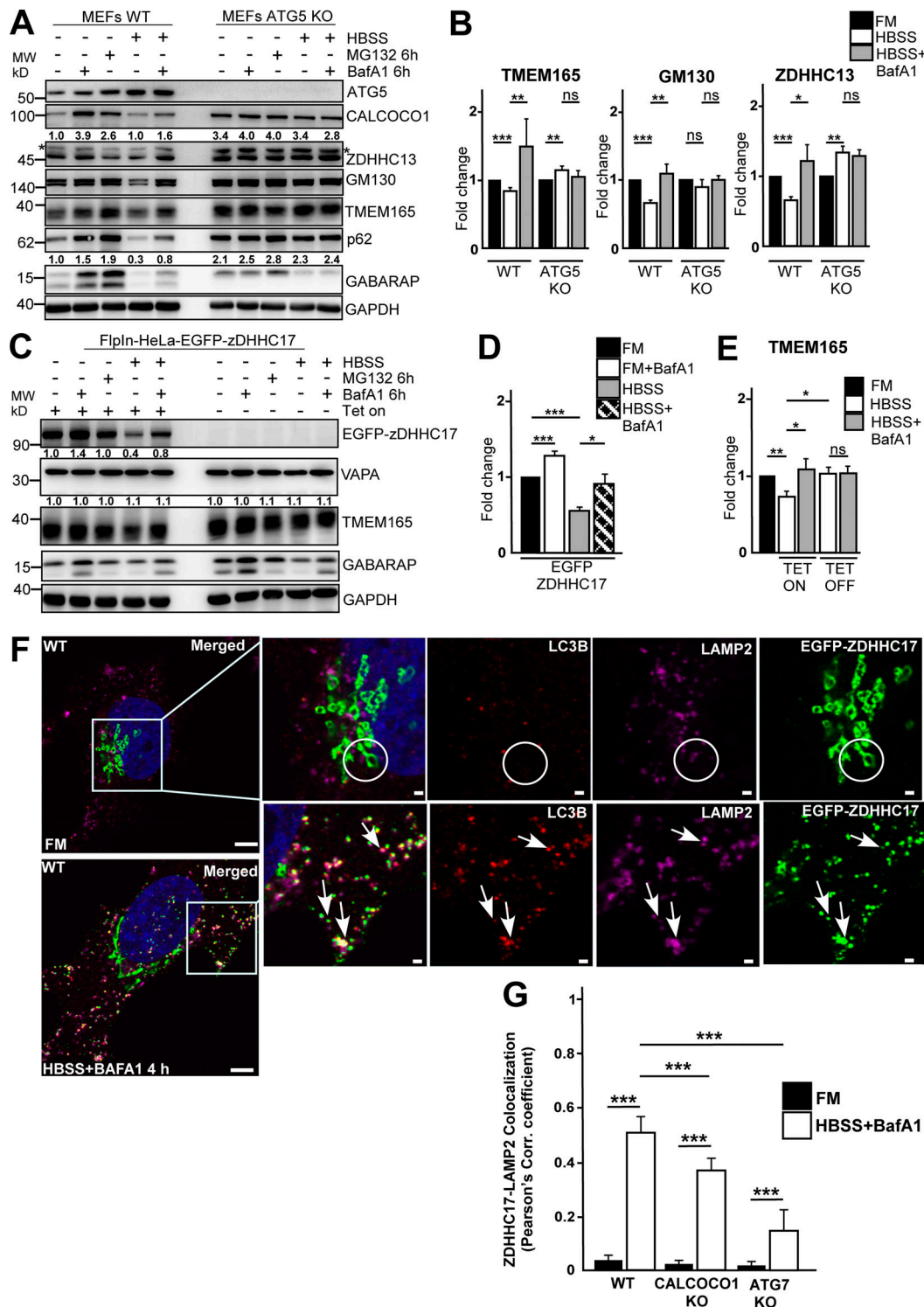
Figure 3. **ZDHHC17 promotes degradation of Golgi by autophagy during starvation. (A and B)** MEF parental and Atg5 KO cells were left untreated, treated with Baf A1 for 6 h or MG132 for 6 h, or starved for 6 h with or without Baf A1. Cell lysates were analyzed by immunoblotting with the indicated antibodies. In A, the panels are collected from more than one Western blot experiment, but for clarity, only a single GAPDH loading control is shown. Numbers below the blots represent relative intensity of the bands in the blots shown, normalized against loading control. The asterisks (*) indicate unspecific bands. The bars in B represent the mean ± SD of band intensities relative to the loading control from three independent experiments quantified using ImageJ. Statistical comparison was analyzed by one-way ANOVA followed by Tukey multiple comparison test. Significance is displayed as ***, P < 0.001; **, P < 0.005; *, P < 0.01. **(C–E)** HeLa cells stably expressing tetracycline-inducible EGFP-ZDHHC17 were left uninduced or induced for 48 h and then treated as in A. Cell lysates were analyzed by immunoblotting with the indicated antibodies. Numbers below the EGFP-ZDHHC17 blot represent relative intensity of the bands normalized against the loading control. Data in D and E are presented as mean ± SD of three independent experiments. Statistical comparison was analyzed as in B; significance is displayed as ***, P < 0.001; **, P < 0.005; *, P < 0.01. **(F)** HeLa WT cells were transfected with EGFP-ZDHHC17; 24 h after transfection, were

either left untreated or starved (HBSS) for 4 h with Baf A1 treatment, then immunostained for endogenous LC3B and LAMP2. The arrows point to colocalization. Bars represent 5 μm (main) and 1 μm (insets). **(G)** Colocalization analysis of EGFP-ZDHHC17 and LAMP2 in WT HeLa cells analyzed in F, CALCOCO1 KO cells analyzed in Fig. S1 D, and ATG7 KO cells analyzed in Fig. S2 D. The error bars represent mean ± SEM of three independent experiments per condition with 100 cells per experiment. Statistical comparison was analyzed by one-way ANOVA followed by Tukey multiple comparison test. Significance is displayed as ***, P < 0.001. MW, molecular weight.

mLIR + Δ623–691 did not promote autophagic degradation of GM130 and TMEM165 during starvation, as indicated by lack of accumulation of the proteins in cells treated with HBSS + BafA1 relative to cells treated with HBSS only (Fig. S3, C and D). This contrasted with the degradation observed in cells expressing WT EGFP-CALCOCO1 (Fig. 5 A), suggesting that the binding to ATG8

proteins was required for CALCOCO1-mediated Golgiphagy. Inducible expression of the monomeric CALCOCO1Δ145–513 (ΔCC) deletion mutant failed to induce degradation of TMEM165 during starvation of CALCOCO1 KO cells (Fig. S3 E). Thus, self-interaction of CALCOCO1 plays a role in Golgiphagy. When CALCOCO1 KO cells were reconstituted with inducible EGFP-CALCOCO1
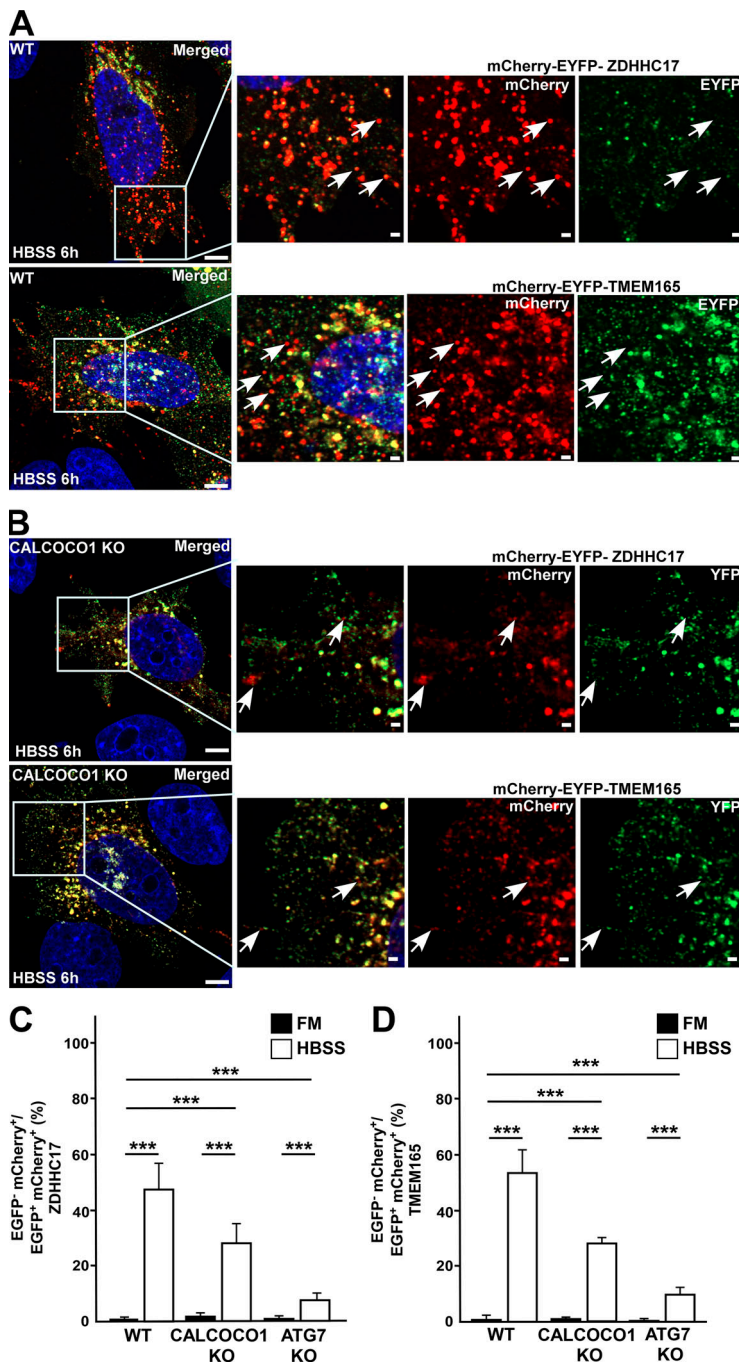
Figure 4. **Depletion of CALCOCO1 decreases Golgi degradation by autophagy. (A and B)** WT (A) and CALCOCO1 KO (B) HeLa cells were transiently transfected with mCherry-EYFP-ZDHHC17 or mCherry-EYFP-TMEM165. 24 h after transfection, the cells were treated or not with HBSS as indicated. The arrows point to red-only puncta. Bars represent 5 μm (main) and 1 μm (insets). **(C and D)** The fraction of red-only puncta in the cells shown in A and B and in ATG7 KO HeLa cells (see Fig. S3 A) were counted and are shown as a percentage of total puncta. The error bars represent mean ± SD of red-only puncta percentages of three independent experiments. Statistical comparison was analyzed by one-way ANOVA followed by Tukey multiple comparison test; significance is displayed as ***, P < 0.001.
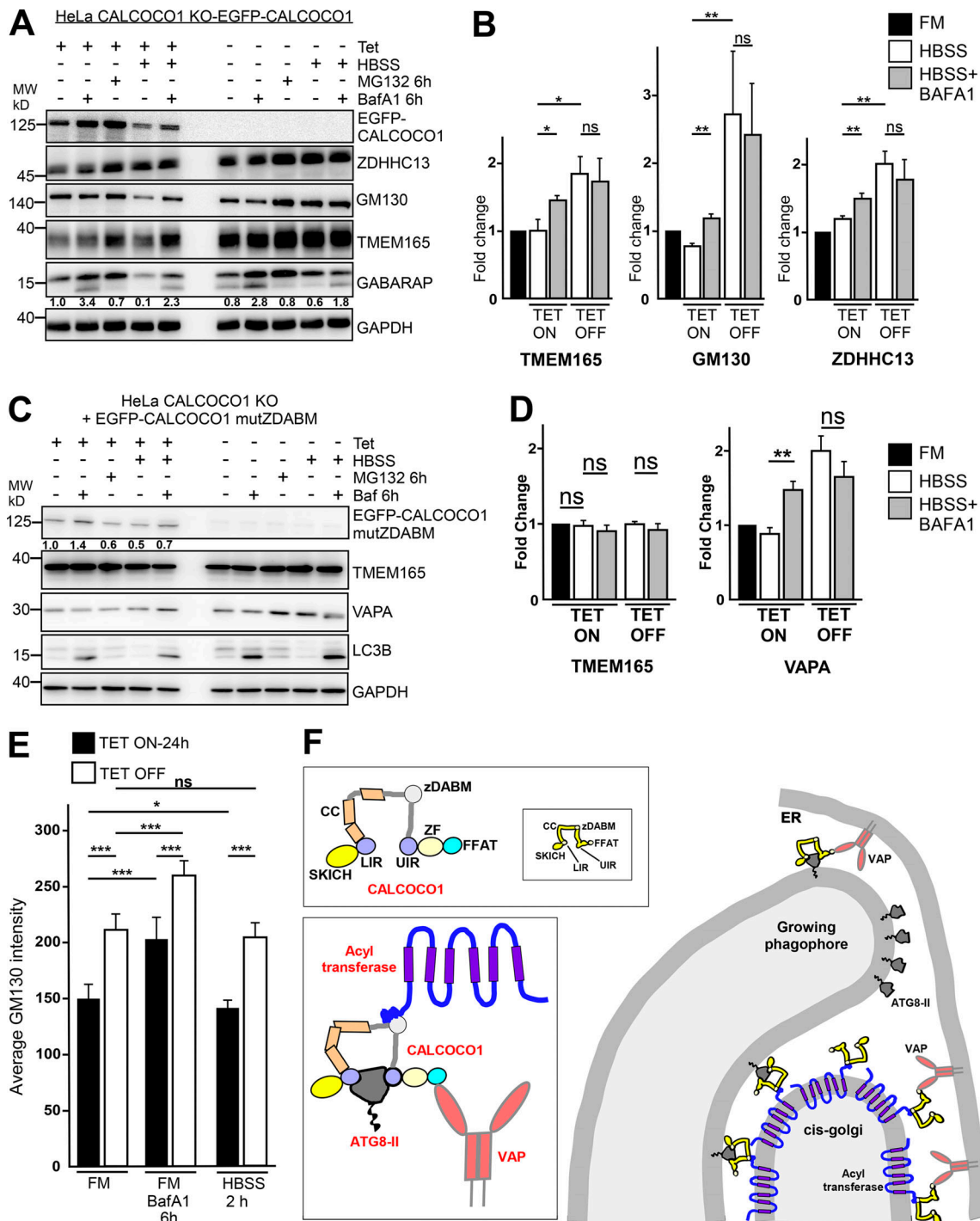
Figure 5. **CALCOCO1 mediates degradation of Golgi by autophagy. (A and B)** HeLa-CALCOCO1 KO cells reconstituted with inducible EGFP-CALCOCO1 were left uninduced or induced for 48 h and then left untreated, treated with Baf A1 for 6 h or MG132 for 6 h, or starved (HBSS) for 6 h with or without Baf A1. Cell lysates were analyzed by immunoblotting with the indicated antibodies. In A, the panels are collected from more than one Western blot experiment, but for clarity, only a single GAPDH loading control is shown. Numbers below the GABARAP blot represent relative intensity of the bands normalized against loading control. The bars in B represent the mean ± SD of band intensities relative to the loading control from three independent experiments quantified using ImageJ. Statistical comparison was analyzed by one-way ANOVA followed by Tukey multiple comparison test. Significance is displayed as **, P < 0.005; *, P < 0.01. **(C and D)** HeLa-CALCOCO1 KO cells reconstituted with EGFP-CALCOCO1-mutZDABM were left uninduced or were induced for 24 h and then either left untreated or treated as indicated. Cell lysates were analyzed by immunoblotting using the indicated antibodies. Numbers below the EGFP-CALCOCO1-mutZDABM blot represent relative intensity of the bands normalized against loading control. The error bars in D represent the mean ± SD of band intensities relative to the loading control from three independent experiments quantified using ImageJ. Statistical comparison was analyzed by one-way ANOVA followed by Tukey multiple comparison test. Significance is displayed as **, P < 0.005. **(E)** HeLa-CALCOCO1 KO cells reconstituted with inducible expression of EGFP-CALCOCO1 were induced for 24 h and then left untreated or treated with Baf A1 or starved for the indicated times. The abundance of the Golgi apparatus was then quantified from wide-field fluorescence images with immunostaining of endogenous GM130, acquired in random fashion. For each condition analyzed, 25

regions of interest (typically containing 1,200–1,800 cells in total) were randomly chosen across each well, and the average fluorescence intensity of GM130-positive structures contained inside the total cell area population of chosen regions was measured. Images were analyzed in Volocity software using a custom-made measurement protocol to segment images into populations of objects representing nuclei, total cell area, and Golgi. The error bars represent mean ± SD of the intensities of GM130-positive structures in the analyzed cells. Statistical comparison was analyzed by one-way ANOVA followed by Tukey multiple comparison test. Significance is displayed as ***, $P < 0.001$; *, $P < 0.01$. **(F)** A model of the CALCOCO1 bridging the gap between the Golgi and autophagic membrane. MW, molecular weight.

Δ671–691, an FFAT-like motif deletion mutant incapable of interacting with the ER-resident VAP proteins, the amount of TMEM165 in the HBSS-only–treated cells was lower in the induced cells than in the noninduced cells (Fig. S3 F). An observable accumulation of the protein in the induced cells also occurred when the cells were treated with HBSS + BafA1, but not in the noninduced cells (Fig. S3 F), suggesting that FFAT-like motif deletion did not block CALCOCO1-mediated Golgiphagy. However, the amounts of VAPA in both HBSS + BafA1– and HBSS-only–treated cells were equal in induced and noninduced cells, suggesting impaired or reduced ER-phagy by the lack of FFAT-like motif in CALCOCO1. Together, these results indicate that the role of CALCOCO1 in ER-phagy is distinct from its role in Golgiphagy. A model of how we envision CALCOCO1 acting as a Golgiphagy receptor via binding to ATG8s and ZDHHC17/13 is shown in Fig. 5 F.

Selective autophagy receptors for degradation of mitochondria, ER, lysosomes, and peroxisomes have been identified (Johansen and Lamark, 2020; Kirkin and Rogov, 2019). In this study, we have identified CALCOCO1 as a selective autophagy receptor for degradation of Golgi membranes and proteins and demonstrated that autophagy is a Golgi remodeling mechanism in response to nutrient starvation. The interaction of CALCOCO1 (and its paralog TAX1BP1) with the Golgi membrane is mediated through binding to the cytoplasmic AR domain of the Golgi transmembrane ZDHHC17 and -13 proteins via an evolutionary conserved zDABM motif, a canonical ZDHHC17/-13 substrate recognition motif, which in CALCOCO1 encompasses the 574-VVISQP-579 core sequence. As large-scale palmitoylation studies have not identified CALCOCO1 as a substrate (Blanc et al., 2015), the involvement of ZDHHC17/-13 in mediating Golgiphagy is likely a palmitoylation-independent function.

Our results suggest that under basal conditions, CALCOCO1, via its zDABM motif, is anchored on the Golgi by ZDHHC17/-13. Nutrient starvation induces disassembly and fragmentation of the Golgi and delivery of the fragments to autophagosomes. This delivery is mediated by ZDHHC17-anchored CALCOCO1 interaction with the autophagy machinery. CALCOCO1, bound to ZDHHC17 on the Golgi membrane, recruits ATG8 proteins via LIR and UIR motifs to initiate autophagosome biogenesis and subsequent degradation of a subset of Golgi proteins in order to maintain Golgi homeostasis (Fig. 5 F). This is consistent with the notion that autophagy receptors act upstream of the core autophagy machinery (Turco et al., 2020). This is supported by our observation that mutant CALCOCO1 lacking both LIR and UIR motifs impaired the turnover of GM130 and TMEM165.

Our data suggest a direct link between the starvation-induced Golgi stress response and CALCOCO1-mediated Golgiphagy. Nutrient starvation induces up-regulation of Golgi

matrix and transmembrane proteins, which are subsequently cleared by CALCOCO1-mediated Golgiphagy. The up-regulation seen is consistent with studies showing that the Golgi stress response due to nutrient starvation, viral infection, or toxic insult caused up-regulation of structural proteins, glycosylation enzymes, and vesicular transport components (Oku et al., 2011; Taniguchi and Yoshida, 2017; Taniguchi et al., 2015). We conclude that CALCOCO1-mediated Golgiphagy is induced by the need to remove excess Golgi components generated during stress in order to restore the pre-stress state of the Golgi. Nutrient starvation is likely not the only trigger for CALCOCO1-mediated Golgiphagy. Bacterial and viral infections and neurodegenerative diseases induce Golgi fragmentation (Campadelli et al., 1993; Gonatas et al., 2006). CALCOCO1 may mediate autophagy-mediated removal of damaged Golgi portions and fragments under these pathological conditions. Our data also suggest involvement of Golgiphagy in the constitutive Golgi turnover and CALCOCO1 in the maintenance of Golgi homeostasis during nutrient-replete conditions. However, ZDHHC17 neither induced significant Golgiphagy nor colocalized significantly with LAMP2 and LC3B under nutrient-replete conditions. Therefore, CALCOCO1-ZDHHC17–dependent degradation may not be involved in the constitutive Golgi turnover during these conditions.

We recently reported a role for CALCOCO1 in ER-phagy, depending on a direct interaction with the ER proteins VAPA and VAPB (Nthiga et al., 2020). Here we show that the ZDHHC17/13–CALCOCO1 interaction is specific for Golgiphagy and is not needed for starvation-induced ER-phagy mediated by CALCOCO1. The discovery that ZDHHC17/-13–CALCOCO1 coupling is involved in the degradation of Golgi components by autophagy is an important step in understanding how autophagy may regulate Golgi homeostasis. Very likely, other selective autophagy receptors may be involved in Golgiphagy. A prime candidate for further studies, TAX1BP1, is indicated in this work.

Materials and methods
Antibodies
Antibodies used were mouse monoclonal anti-CALCOCO1 (A-10; sc-515670; Santa Cruz Biotech), rabbit polyclonal anti-CALCOCO1 (HPA038314; Sigma-Aldrich), rabbit polyclonal anti-ZDHHC13 (24759-1-AP; Proteintech), rabbit polyclonal anti-ZDHHC17 (15465-1-AP; Proteintech), rabbit polyclonal anti-TMEM165 (20485-1-AP; Proteintech), rabbit polyclonal anti-GFP (ab290; Abcam), mouse monoclonal anti-p62 (610833; BD Biosciences), guinea pig polyclonal anti-p62 (GP62-C; Progen), rabbit monoclonal anti-ATG7 (D12B11; Cell Signaling), rabbit polyclonal anti-LC3B (NB100-2220; Novus Bio), rabbit polyclonal anti-LC3B

(L7543; Sigma-Aldrich), mouse monoclonal anti-GABARAP (M135-3; MBL), mouse monoclonal anti-Myc tag clone 9B11 (2276; Cell Signaling), mouse anti-LAMP2 (sc-18822; Santa Cruz Biotech), rabbit polyclonal anti-VAPA (15275-1-AP; Proteintech), rabbit anti-ATG5 (12994; Cell Signaling), rabbit monoclonal anti-ATG7 (D12B11; Cell Signaling), rabbit monoclonal anti-GM130 (52649; Abcam), rabbit polyclonal anti-GAPDH (G9545; Sigma-Aldrich), rabbit polyclonal anti-actin (A2066; Sigma-Aldrich), HRP-conjugated goat polyclonal anti-rabbit (554021; BD Biosciences), and HRP-conjugated goat polyclonal anti-mouse (554002; BD Biosciences).

Reagents/chemicals
Reagents and chemicals used were BafA1 (sc-201550; Santa Cruz Biotech), MG132 (C2211; Sigma-Aldrich), [^{35}S]methionine (NEG709-A500UC; PerkinElmer), T7-coupled reticulocyte lysate system (14610; Promega), Ponceau S (P3504; Sigma-Aldrich), DMEM (D6046; Sigma-Aldrich), bicarbonate buffered HBSS (H9269; Sigma-Aldrich), Hygromycin (10687-010; Thermo Fisher Scientific), tetracycline (87128; Sigma-Aldrich), penicillin/streptomycin (P4333; Sigma-Aldrich), Metafectene Pro (T040; Biontex), (S0615; Biochrom), Lipofectamine RNAiMAX (13778; Thermo Fisher Scientific), cOmplete EDTA-free Protease inhibitor (11836170001; Roche), chemiluminescent HRP substrate (Sigma-Aldrich), and glutathione sepharose beads (17-5132-01; GE Healthcare).

Plasmid constructs
All the plasmid constructs used in this study are listed in Table 1. The constructs were made using conventional cloning techniques and the Gateway recombination system (Invitrogen). Mutagenesis was performed using the QuickChange site-directed mutagenesis kit (Stratagene). Oligonucleotides for mutagenesis and sequencing were from Invitrogen. All constructs were verified by sequencing (BigDye, Applied Biosystems). pDONR201-CALCOCO1 (HSCD00081507), pENTR223-ZDHHC13 (HsCD00376338), and PENTR223-ZDHHC17 (HsCD00377094) were obtained from Harvard plasmid collection. pCR4-TOPO-TMEM165 was obtained from Dharmacon (ID 8143983)

Mammalian cell culture and cell treatments
We used human HeLa cells (ATCC CCL-2), MEFs, Atg5 KO MEFs (Kuma et al., 2004), and CRISPR-Cas9–generated HeLa ATG7 KO cells (Mejlvang et al., 2018). All cells were cultured in DMEM (D6046; Sigma-Aldrich) supplemented with 10% FBS (S0615; Biochrom) and 1% streptomycin-penicillin (P4333; Sigma-Aldrich) and kept in a humidified incubator at 37°C and 5% CO_2. Starvation experiments were conducted by incubating cells in HBSS (H9269; Sigma-Aldrich). Cells were treated with 1 μg/ml tetracycline (Sigma-Aldrich), 200 ng/ml BafA1 (sc-201550; Santa Cruz Biotechnology), and 25 μM MG132 for the indicated time periods. DNA transfection was done with Metafectene Pro (T040; Biontex) according to the manufacturer's protocol. siRNA transfections were done with RNAiMAX according to the manufacturer's protocol.

Generation and propagation of inducible stable cell lines
Flp-In Trex HeLa cells and Flp-In Trex HEK293 cells were used to create inducible stable cell lines and to produce CALCOCO1 KO

Table 1. **Plasmids used in the study**

Plasmid	Reference
pDONOR221-CALCOCO1	Nthiga et al., 2020
pDONOR221-CALCOCO1 ΔLIRΔ623–691	Nthiga et al., 2020
pDONOR221-CALCOCO1 (574-VVISQP/574-AAISAA)	This study
pDest-FlpIn-EGFP-CALCOCO1 (574-VVISQP/574-AAISAA)	This study
pDest-FlipIn-EGFP-CALCOCO1 Δ671–691	This study
pDest-MYC-CALCOCO1	Nthiga et al., 2020
pDest-MYC-CALCOCO1 (574-VVISQP/574-AAISAA)	This study
pDest-EGFP-C1	Lamark et al., 2003
pDest-EGFP-CALCOCO1	Nthiga et al., 2020
pDest-FlpIn-EGFP-CALCOCO1	Nthiga et al., 2020
pDONOR221-TAX1BP1	This study
pDONOR221-TAX1BP1 Δ673–679	This study
pDest-MYC-TAX1BP1	This study
pDest-MYC-TAX1BP1 Δ673–679	This study
pDONOR221-ZDHHC13	This study
pDest-EGFP-ZDHHC13	This study
pDONOR221-ZDHHC17	This study
pDONOR221-ZDHHC17 (N100A/W130A)	This study
pDest-FlpIn-EGFP-ZDHHC17 (N100A/W130A)	This study
pDest-EGFP-ZDHHC17	This study
pDest-FlpIn-EGFP-ZDHHC17	This study
pDest-mCherry-EYFP-ZDHHC17	This study
pDest15-C1	Lamark et al., 2003
pDest15-ZDHHC17	This study
pDest15-ZDHHC17 (N100A/W130A)	This study
pDONOR221-TMEM615	This study
pDest-mCherry-EYFP-TMEM165	This study

cells. Tagged constructs were cloned into pcDNA5/FRT/TO vector using the Gateway technology and then cotransfected with recombinase pOG44 into the Flp-In Trex cells. After 48 h, colonies of cells with the gene of interest integrated into the flippase recognition target site were selected with 200 μg/ml hygromycin (400051; Calbiochem) and 7.5 μg/ml blasticidin. Polyclonal hygromycin-resistant cells were then expanded in the selection medium and later tested for expression by immunoblotting and immunofluorescence. The expression of the gene was induced with 1 μg/ml tetracycline for 24 h.

Generation of KO cell lines using CRISPR-Cas9
The generation of CALCOCO1 KO HeLa cells has been described previously (Nthiga et al., 2020). Briefly, specific gRNAs were designed using the CHOPCHOP web tool (https://chopchop.cbu.uib.no; Labun et al., 2019). The sequence of the sgRNA used was 5′-CACCGGAAGAATCACCACTAAGCC-3′. The sense and antisense oligonucleotides were annealed and phosphorylated and then ligated into a BbsI linearized pSpCas9(BB)-2A-Puro

(PX459) vector (62988; Addgene). To generate CALCOCO1 KO, Flp-In T-Rex HeLa cells were transfected with the PX459 vector containing sgRNA targeting exon 2 using Metafectene Pro. 24 h after transfection, the cells were selected by treatment with puromycin at 1 µg/ml for 72 h. Puromycin-resistant cells were then singly sorted into 96-well plates, and the clones were expanded and screened by immunoblotting. Once KO was confirmed by immunoblotting, genomic DNA was extracted, and the area of interest was amplified by PCR. The amplified region was ligated into the PGEM vector (A3600; Promega) and sequenced to identify the indels. The generation of ATG7 KO HeLa cells has been described previously (Mejlvang et al., 2018)

Western blotting

Cells were directly lysed in 2× Laemmli buffer (50 mM Tris, pH 7.4, 2% SDS, 10% glycerol, and 200 mM DTT [D0632; Sigma-Aldrich]) and heated for 10 min. Protein concentrations were measured by Pierce BCA Protein Assay Kit (23227; Thermo Fisher Scientific), and 30–40 µg protein of the sample was resolved by SDS-PAGE and transferred to nitrocellulose membrane. Membranes were blocked in PBS or TBS containing 0.1% Tween and 5% lowfat milk and then incubated overnight at 4°C with the indicated primary antibodies in the blocking solution. Immunoblot bands were quantified using ImageJ.

Mass spectrometry (MS)

Gel pieces were subjected to in-gel reduction, alkylation, and tryptic digestion using 6 ng/µl trypsin (V511A; Promega). OMIX C18 tips (Varian) were used for sample cleanup and concentration. Peptide mixtures containing 0.1% formic acid were loaded onto a Thermo Fisher Scientific EASY-nLC1000 system and EASY-Spray column (C18, 2 µm, 100 Å, 50 µm, 50 cm). Peptides were fractionated using a 2–100% acetonitrile gradient in 0.1% formic acid over 50 min at a flow rate of 200 nl/min. The separated peptides were analyzed using a Thermo Fisher Scientific Q-Exactive mass spectrometer. Data were collected in data-dependent mode using a Top10 method. The raw data were processes using MaxQuant software v1.6.0.16 using the label-free quantification method. MS/MS data were searched against a Uniprot human database. A false discovery rate of 0.01 was needed to give a protein identification. Perseus v1.6.0.7 was used for statistical analysis.

GST pulldown assays

GST-fusion proteins (LC3s, GABARAPs, CALCOCO1, and ZDHHC17) were expressed in *Escherichia coli* SoluBL21 (DE3; C700200; Genlantis) in Luria-Bertani broth medium. Protein expression was induced by addition of 0.5 mM IPTG, and cells were incubated with shaking at 37°C for 4 h. Harvested cells were sonicated in the lysis buffer (20 mM Tris-HCl, pH 7.5, 10 mM EDTA, 5 mM EGTA, and 150 mM NaCl), and the GST-fused proteins were then immobilized on glutathione Sepharose 4 Fast Flow beads (17-5132-01; GE Healthcare) by incubating in a rotator at 4°C for 1 h. Fusion protein-bound beads were then used directly in GST pull-down assays with in vitro–translated proteins. In vitro translation was done in the presence of radioactive [^{35}S]methionine using the TNT T7 Reticulocyte Lysate System (14610; Promega). 12 µl of the in vitro–translated protein was then precleared by incubation with 10 µl of empty glutathione Sepharose beads in 100 µl NETN buffer (50 mM Tris, pH 8.0, 150 mM NaCl, 1 mM EDTA, and 0.5% NP-40) supplemented with cOmplete Mini EDTA-free protease inhibitor for 30 min at 4°C to remove nonspecific binding. The precleared lysates were incubated with the GST fusion protein–loaded beads for 1 h at 4°C. The beads were washed five times with NETN buffer, followed by resuspension in sample loading buffer (100 mM Tris, pH 7.4, 4% SDS, 20% glycerol, 0.2% bromophenol blue, and 200 mM DTT), boiled for 10 min, and resolved in SDS-PAGE. Gels were stained with Coomassie Brilliant Blue R-250 Dye (20278; Thermo Fisher Scientific) for 30 min to visualize the fusion proteins, washed, and vacuum-dried (in Saskia HochVakuum combined with Bio-Rad Gel dryer model 583; 1651746) for 30 min. Radioactive signals were analyzed by Fujifilm bioimaging analyzer BAS-5000 (Fujifilm).

Immunofluorescence

Cells were plated on glass coverslips (631-0150; VWR) or in Lab-Tek chambered coverglass (155411; Thermo Fisher Scientific), fixed in 4% (wt/vol) formaldehyde for 10 min at room temperature, permeabilized with 0.1% Triton X-100 in PBS at room temperature for 5 min, and blocked in PBS containing 3% goat serum for 1 h at room temperature. Cells were then incubated overnight at 4°C with primary antibody diluted in PBS containing 2% goat serum. After five washes in PBS, they were incubated with Alexa Fluor secondary antibodies in PBS containing 2% goat serum for 1 h at room temperature, followed by five washes in PBS. Nuclei were stained with 1 µg/ml DAPI in PBS for 10 min, followed by one final wash in PBS. Coverslips were mounted in 10 µl of Mowiol and placed on a glass microscope slide.

Light microscopy

Cells were imaged on an Observer Z.1 inverted microscope, equipped either with an LSM780/LSM880 scanner for confocal microscopy or an Axiocam 506 monochromatic camera for wide-field microscopy, followed by deconvolution (both systems Carl Zeiss Microscopy). Images were collected in Zen software using a 63× NA 1.4 oil-immersion lens for coverslips or a 40× NA 1.2 water-immersion lens for chambered coverglass. Optimal excitation and emission settings were determined using the Smart Setup function. For deconvolution microscopy, z-stacks were obtained with 0.1-µm step size and without camera binning, resulting in a lateral pixel spacing of 0.114 µm. Images were deconvolved in Huygens (Scientific Volume Imaging) v19.04 using the classic maximum likelihood estimation algorithm with built-in theoretical point spread functions for each fluorophore. All fluorescence channels were recorded at nonsaturating levels, and settings were kept identical between all samples used for comparisons or quantifications.

Image analysis

The abundance of the Golgi apparatus was quantified from wide-field fluorescence images of endogenous GM130, acquired in random fashion using the Tiles & Positions module of Zen. For

each condition analyzed, 25 regions of interest (typically containing, 1,200–1,800 cells in total) were randomly distributed across each well. Cells were autofocused in the DAPI channel, and images were acquired with identical illumination and camera settings between wells. Images were analyzed in Volocity (PerkinElmer) v6.3 using a custom-made measurement protocol to segment images into populations of objects representing nuclei, total cell area, and Golgi. To quantify changes in Golgi abundance, the average fluorescence intensity of GM130-positive structures contained inside the total cell area population was measured for all images, and the average intensity was reported for each treatment group.

Online supplemental material

Fig. S1 shows colocalization of EGFP-CALCOCO1 and Myc-ZDHHC17 or Myc-ZDHHC13 on Golgi structures in transfected HeLa cells, and that this colocalization is strongly reduced by a point mutation affecting the zDABM motif in CALCOCO1. Fig. S2 shows that Golgiphagy during starvation requires macroautophagy and depends on the ZDHHC17–CALCOCO1 interaction. Fig. S3 shows that CALCOCO1-mediated Golgiphagy depends on ATG7 and the ATG8 interaction motifs, but not on the VAP interacting FFAT-like motif.

References

Birgisdottir, A.B., T. Lamark, and T. Johansen. 2013. The LIR motif - crucial for selective autophagy. *J. Cell Sci.* 126:3237–3247.

Blanc, M., F. David, L. Abrami, D. Migliozzi, F. Armand, J. Bürgi, and F.G. van der Goot. 2015. SwissPalm: Protein Palmitoylation database. *F1000 Res.* 4:261. https://doi.org/10.12688/f1000research.6464.1

Campadelli, G., R. Brandimarti, C. Di Lazzaro, P.L. Ward, B. Roizman, and M.R. Torrisi. 1993. Fragmentation and dispersal of Golgi proteins and redistribution of glycoproteins and glycolipids processed through the Golgi apparatus after infection with herpes simplex virus 1. *Proc. Natl. Acad. Sci. USA.* 90:2798–2802. https://doi.org/10.1073/pnas.90.7.2798

Dikic, I., and Z. Elazar. 2018. Mechanism and medical implications of mammalian autophagy. *Nat. Rev. Mol. Cell Biol.* 19:349–364. https://doi.org/10.1038/s41580-018-0003-4

Ernst, A.M., S.A. Syed, O. Zaki, F. Bottanelli, H. Zheng, M. Hacke, Z. Xi, F. Rivera-Molina, M. Graham, A.A. Rebane, et al. 2018. S-Palmitoylation Sorts Membrane Cargo for Anterograde Transport in the Golgi. *Dev. Cell.* 47:479–493.e7. https://doi.org/10.1016/j.devcel.2018.10.024

Farquhar, M.G. 1985. Progress in unraveling pathways of Golgi traffic. *Annu. Rev. Cell Biol.* 1:447–488. https://doi.org/10.1146/annurev.cb.01.110185.002311

Feng, Y., D. He, Z. Yao, and D.J. Klionsky. 2014. The machinery of macroautophagy. *Cell Res.* 24:24–41. https://doi.org/10.1038/cr.2013.168

Fukata, Y., and M. Fukata. 2010. Protein palmitoylation in neuronal development and synaptic plasticity. *Nat. Rev. Neurosci.* 11:161–175. https://doi.org/10.1038/nrn2788

Gonatas, N.K., A. Stieber, and J.O. Gonatas. 2006. Fragmentation of the Golgi apparatus in neurodegenerative diseases and cell death. *J. Neurol. Sci.* 246:21–30. https://doi.org/10.1016/j.jns.2006.01.019

Hübner, C.A., and I. Dikic. 2020. ER-phagy and human diseases. *Cell Death Differ.* 27:833–842. https://doi.org/10.1038/s41418-019-0444-0

Johansen, T., and T. Lamark. 2011. Selective autophagy mediated by autophagic adapter proteins. *Autophagy.* 7:279–296. https://doi.org/10.4161/auto.7.3.14487

Johansen, T., and T. Lamark. 2020. Selective Autophagy: ATG8 Family Proteins, LIR Motifs and Cargo Receptors. *J. Mol. Biol.* 432:80–103. https://doi.org/10.1016/j.jmb.2019.07.016

Kirkin, V., and V.V. Rogov. 2019. A Diversity of Selective Autophagy Receptors Determines the Specificity of the Autophagy Pathway. *Mol. Cell.* 76:268–285. https://doi.org/10.1016/j.molcel.2019.09.005

Kuma, A., M. Hatano, M. Matsui, A. Yamamoto, H. Nakaya, T. Yoshimori, Y. Ohsumi, T. Tokuhisa, and N. Mizushima. 2004. The role of autophagy during the early neonatal starvation period. *Nature.* 432:1032–1036. https://doi.org/10.1038/nature03029

Labun, K., T.G. Montague, M. Krause, Y.N. Torres Cleuren, H. Tjeldnes, and E. Valen. 2019. CHOPCHOP v3: expanding the CRISPR web toolbox beyond genome editing. *Nucleic Acids Res.* 47(W1):W171–W174. https://doi.org/10.1093/nar/gkz365

Lemonidis, K., R. MacLeod, G.S. Baillie, and L.H. Chamberlain. 2017. Peptide array-based screening reveals a large number of proteins interacting with the ankyrin-repeat domain of the zDHHC17 S-acyltransferase. *J. Biol. Chem.* 292:17190–17202. https://doi.org/10.1074/jbc.M117.799650

Lamark, T., M. Perander, H. Outzen, K. Kristiansen, A. Øvervatn, E. Michaelsen, G. Bjørkøy, and T. Johansen. 2003. Interaction codes within the family of mammalian Phox and Bem1p domain-containing proteins. *J. Biol. Chem.* 278:34568–34581. . https://doi.org/10.1074/jbc.M303221200

Lemonidis, K., M.C. Sanchez-Perez, and L.H. Chamberlain. 2015. Identification of a Novel Sequence Motif Recognized by the Ankyrin Repeat Domain of zDHHC17/13 S-Acyltransferases. *J. Biol. Chem.* 290:21939–21950. https://doi.org/10.1074/jbc.M115.657668

Linder, M.E., and R.J. Deschenes. 2007. Palmitoylation: policing protein stability and traffic. *Nat. Rev. Mol. Cell Biol.* 8:74–84. https://doi.org/10.1038/nrm2084

Lu, L.-Q., M.-Z. Tang, Z.-H. Qi, S.-F. Huang, Y.-Q. He, D.-K. Li, L.-F. Li, and L.-X. Chen. 2020. Regulation of the Golgi apparatus via GOLPH3-mediated new selective autophagy. *Life Sci.* 253:117700. https://doi.org/10.1016/j.lfs.2020.117700

Lystad, A.H., and A. Simonsen. 2019. Mechanisms and Pathophysiological Roles of the ATG8 Conjugation Machinery. *Cells.* 8:973. https://doi.org/10.3390/cells8090973

Maeda, S., C. Otomo, and T. Otomo. 2019. The autophagic membrane tether ATG2A transfers lipids between membranes. *eLife.* 8:e45777. https://doi.org/10.7554/eLife.45777

Maeda, S., H. Yamamoto, L.N. Kinch, C.M. Garza, S. Takahashi, C. Otomo, N.V. Grishin, S. Forli, N. Mizushima, and T. Otomo. 2020. Structure, lipid scrambling activity and role in autophagosome formation of ATG9A. *Nat. Struct. Mol. Biol.* 27:1194–1201. https://doi.org/10.1038/s41594-020-00520-2

Marshall, R.S., Z. Hua, S. Mali, F. McLoughlin, and R.D. Vierstra. 2019. ATG8-Binding UIM Proteins Define a New Class of Autophagy Adaptors and Receptors. *Cell.* 177:766–781.e24. https://doi.org/10.1016/j.cell.2019.02.009

Matoba, K., T. Kotani, A. Tsutsumi, T. Tsuji, T. Mori, D. Noshiro, Y. Sugita, N. Nomura, S. Iwata, Y. Ohsumi, et al. 2020. Atg9 is a lipid scramblase that mediates autophagosomal membrane expansion. *Nat. Struct. Mol. Biol.* 27:1185–1193. https://doi.org/10.1038/s41594-020-00518-w

Mejlvang, J., H. Olsvik, S. Svenning, J.-A. Bruun, Y.P. Abudu, K.B. Larsen, A. Brech, T.E. Hansen, H. Brenne, T. Hansen, et al. 2018. Starvation induces rapid degradation of selective autophagy receptors by endosomal

microautophagy. *J. Cell Biol.* 217:3640–3655. https://doi.org/10.1083/jcb .201711002

Nthiga, T.M., B. Kumar Shrestha, E. Sjøttem, J.-A. Bruun, K. Bowitz Larsen, Z. Bhujabal, T. Lamark, and T. Johansen. 2020. CALCOCO1 acts with VAMP-associated proteins to mediate ER-phagy. *EMBO J.* 39:e103649. https://doi.org/10.15252/embj.2019103649

Ohno, Y., A. Kihara, T. Sano, and Y. Igarashi. 2006. Intracellular localization and tissue-specific distribution of human and yeast DHHC cysteine-rich domain-containing proteins. *Biochim. Biophys. Acta.* 1761:474–483. https://doi.org/10.1016/j.bbalip.2006.03.010

Ohsumi, Y. 2014. Historical landmarks of autophagy research. *Cell Res.* 24: 9–23. https://doi.org/10.1038/cr.2013.169

Oku, M., S. Tanakura, A. Uemura, M. Sohda, Y. Misumi, M. Taniguchi, S. Wakabayashi, and H. Yoshida. 2011. Novel cis-acting element GASE regulates transcriptional induction by the Golgi stress response. *Cell Struct. Funct.* 36:1–12. https://doi.org/10.1247/csf.10014

Osawa, T., T. Kotani, T. Kawaoka, E. Hirata, K. Suzuki, H. Nakatogawa, Y. Ohsumi, and N.N. Noda. 2019. Atg2 mediates direct lipid transfer between membranes for autophagosome formation. *Nat. Struct. Mol. Biol.* 26:281–288. https://doi.org/10.1038/s41594-019-0203-4

Pankiv, S., T.H. Clausen, T. Lamark, A. Brech, J.A. Bruun, H. Outzen, A. Øvervatn, G. Bjørkøy, and T. Johansen. 2007. p62/SQSTM1 binds directly to Atg8/LC3 to facilitate degradation of ubiquitinated protein aggregates by autophagy. *J. Biol. Chem.* 282:24131–24145. https://doi.org/10.1074/jbc.M702824200

Rogov, V., V. Dötsch, T. Johansen, and V. Kirkin. 2014. Interactions between autophagy receptors and ubiquitin-like proteins form the molecular basis for selective autophagy. *Mol. Cell.* 53:167–178. https://doi.org/10 .1016/j.molcel.2013.12.014

Sanders, S.S., J. Hou, L.M. Sutton, V.C. Garside, K.K.N. Mui, R.R. Singaraja, M.R. Hayden, and P.A. Hoodless. 2015. Huntingtin interacting proteins 14 and 14-like are required for chorioallantoic fusion during early placental development. *Dev. Biol.* 397:257–266. https://doi.org/10.1016/j .ydbio.2014.11.018

Sasaki, K., and H. Yoshida. 2015. Organelle autoregulation-stress responses in the ER, Golgi, mitochondria and lysosome. *J. Biochem.* 157:185–195. https://doi.org/10.1093/jb/mvv010

Takahashi, Y., C.L. Meyerkord, T. Hori, K. Runkle, T.E. Fox, M. Kester, T.P. Loughran, and H.-G. Wang. 2011. Bif-1 regulates Atg9 trafficking by mediating the fission of Golgi membranes during autophagy. *Autophagy.* 7:61–73. https://doi.org/10.4161/auto.7.1.14015

Taniguchi, M., and H. Yoshida. 2017. TFE3, HSP47, and CREB3 Pathways of the Mammalian Golgi Stress Response. *Cell Struct. Funct.* 42:27–36. https://doi.org/10.1247/csf.16023

Taniguchi, M., S. Nadanaka, S. Tanakura, S. Sawaguchi, S. Midori, Y. Kawai, S. Yamaguchi, Y. Shimada, Y. Nakamura, Y. Matsumura, et al. 2015. TFE3 is a bHLH-ZIP-type transcription factor that regulates the mammalian Golgi stress response. *Cell Struct. Funct.* 40:13–30. https://doi .org/10.1247/csf.14015

Turco, E., D. Fracchiolla, and S. Martens. 2020. Recruitment and Activation of the ULK1/Atg1 Kinase Complex in Selective Autophagy. *J. Mol. Biol.* 432: 123–134. https://doi.org/10.1016/j.jmb.2019.07.027

Valverde, D.P., S. Yu, V. Boggavarapu, N. Kumar, J.A. Lees, T. Walz, K.M. Reinisch, and T.J. Melia. 2019. ATG2 transports lipids to promote autophagosome biogenesis. *J. Cell Biol.* 218:1787–1798. https://doi.org/10 .1083/jcb.201811139

Verardi, R., J.-S. Kim, R. Ghirlando, and A. Banerjee. 2017. Structural Basis for Substrate Recognition by the Ankyrin Repeat Domain of Human DHHC17 Palmitoyltransferase. *Structure.* 25:1337–1347.e6. https://doi .org/10.1016/j.str.2017.06.018

Wilkinson, S. 2019. ER-phagy: shaping up and destressing the endoplasmic reticulum. *FEBS J.* 286:2645–2663. https://doi.org/10.1111/febs.14932

Yu, L., Y. Chen, and S.A. Tooze. 2018. Autophagy pathway: Cellular and molecular mechanisms. *Autophagy.* 14:207–215. https://doi.org/10.1080/ 15548627.2017.1378838

Zaffagnini, G., and S. Martens. 2016. Mechanisms of Selective Autophagy. *J. Mol. Biol.* 428(9, 9 Pt A):1714–1724. https://doi.org/10.1016/j.jmb.2016 .02.004
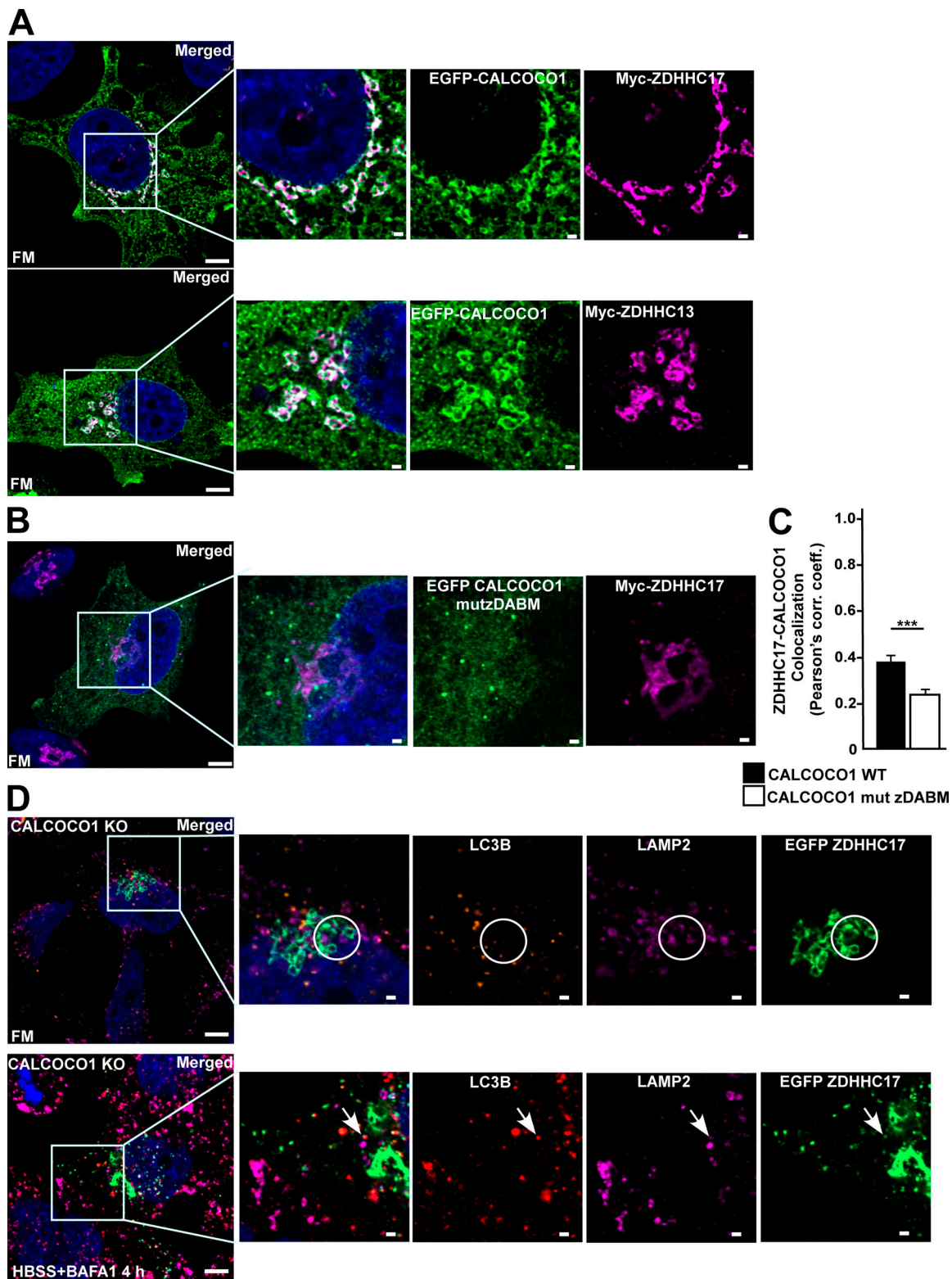
Supplemental material

Figure S1. **Mutation of zDABM motif of CALCOCO1 reduces its Golgi localization. (A)** HeLa cells were cotransfected with EGFP-CALCOCO1 and either Myc-ZDHHC17 or Myc-ZDHHC13, grown in full medium and imaged by confocal microscopy. Bars represent 5 µm (main) and 1 µm (insets). **(B)** HeLa cells were cotransfected with EGFP-CALCOCO-mutZDABM and Myc-ZDHHC17 and then treated as in A. Bars represent 5 µm (main) and 1 µm (insets). **(C)** Colocalization analysis of Myc-ZDHHC17 and EGFP-CALCOCO1 in the cells analyzed in A and B. The error bars represent mean ± SEM of three independent experiments per condition with 100 cells per experiment. Statistical comparison was analyzed by one-way ANOVA followed by Tukey multiple comparison test. Significance is displayed as ***, P < 0.001. corr. coeff., correlation coefficient. **(D)** HeLa CALCOCO1 KO cells were transfected with EGFP-ZDHHC17; 24 h after transfection, they were either left untreated or starved (HBSS) for 4 h with Baf A1 treatment, and then immunostained for endogenous LC3B and LAMP2. The arrows point to colocalization. Bars represent 5 µm (main) and 1 µm (insets).
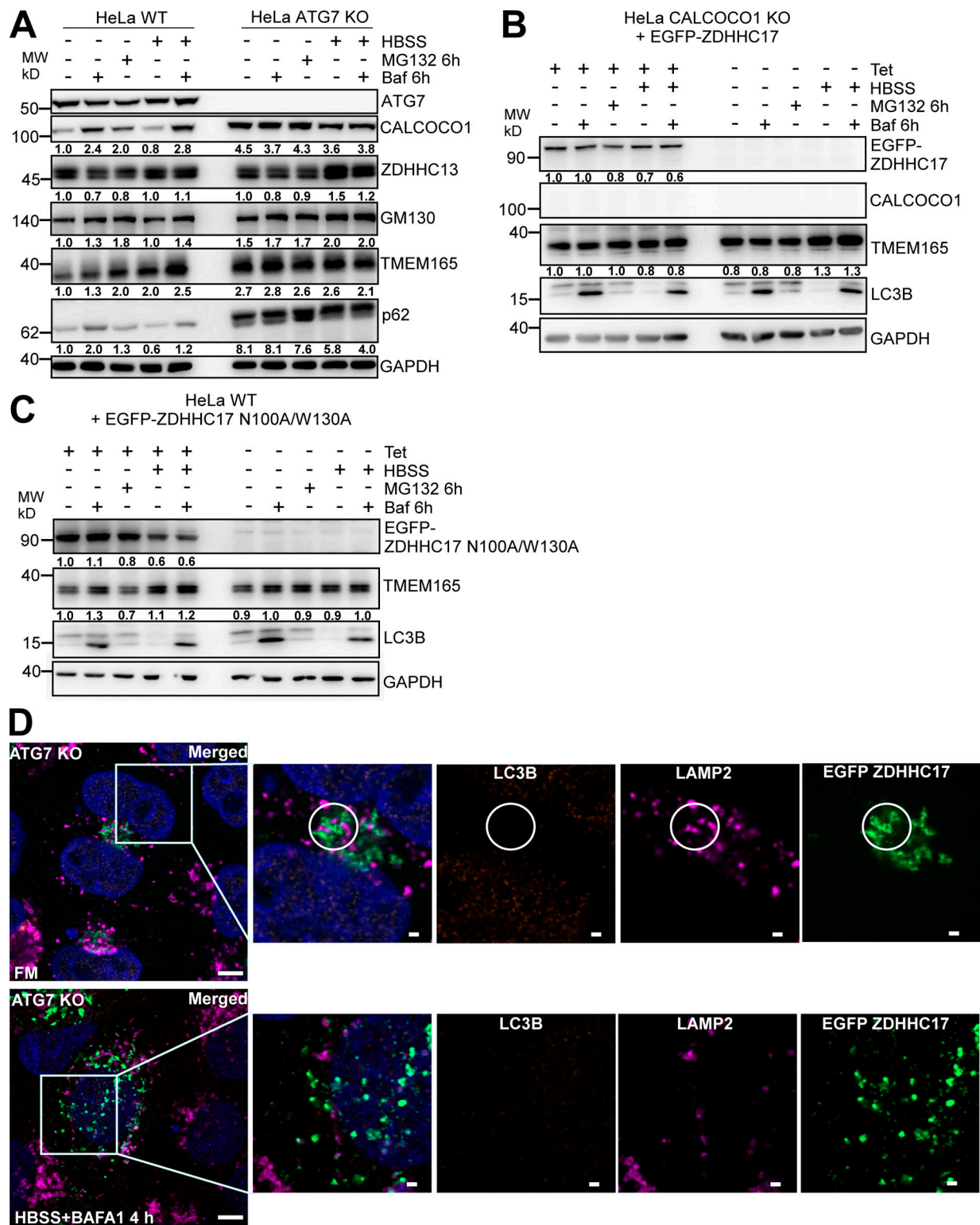
Figure S2. **Golgiphagy during starvation requires macroautophagy and depends on the ZDHHC17-CALCOCO1 interaction. (A)** HeLa parental or ATG7 KO cells were left untreated, treated with either Baf A1 for 6 h or MG132 for 6 h, or starved for 6 h with or without Baf A1. Cell lysates were analyzed by immunoblotting with the indicated antibodies. The panels are collected from more than one Western blot experiment, but for clarity, only a single GAPDH loading control is shown. Numbers below the blots represent relative intensity of the bands in the blots shown, normalized against loading control. **(B and C)** HeLa CALCOCO1 KO cells stably expressing inducible EGFP-ZDHHC17 (B) or EGFP-ZDHHC17 N100A/W130A (C) were left uninduced or induced for 24 h and then left untreated or treated as indicated. Cell lysates were analyzed by immunoblotting with the indicated antibodies. Numbers below the EGFP-ZDHHC17 blot represent relative intensity of the bands normalized against the loading control. **(D)** ATG7 KO HeLa cells were transfected with EGFP-ZDHHC17; 24 h after transfection, they were either left untreated or starved (HBSS) for 4 h with Baf A1 treatment, then immunostained for endogenous LC3B and LAMP2. Bars represent 5 µm (main) and 1 µm (insets). MW, molecular weight.
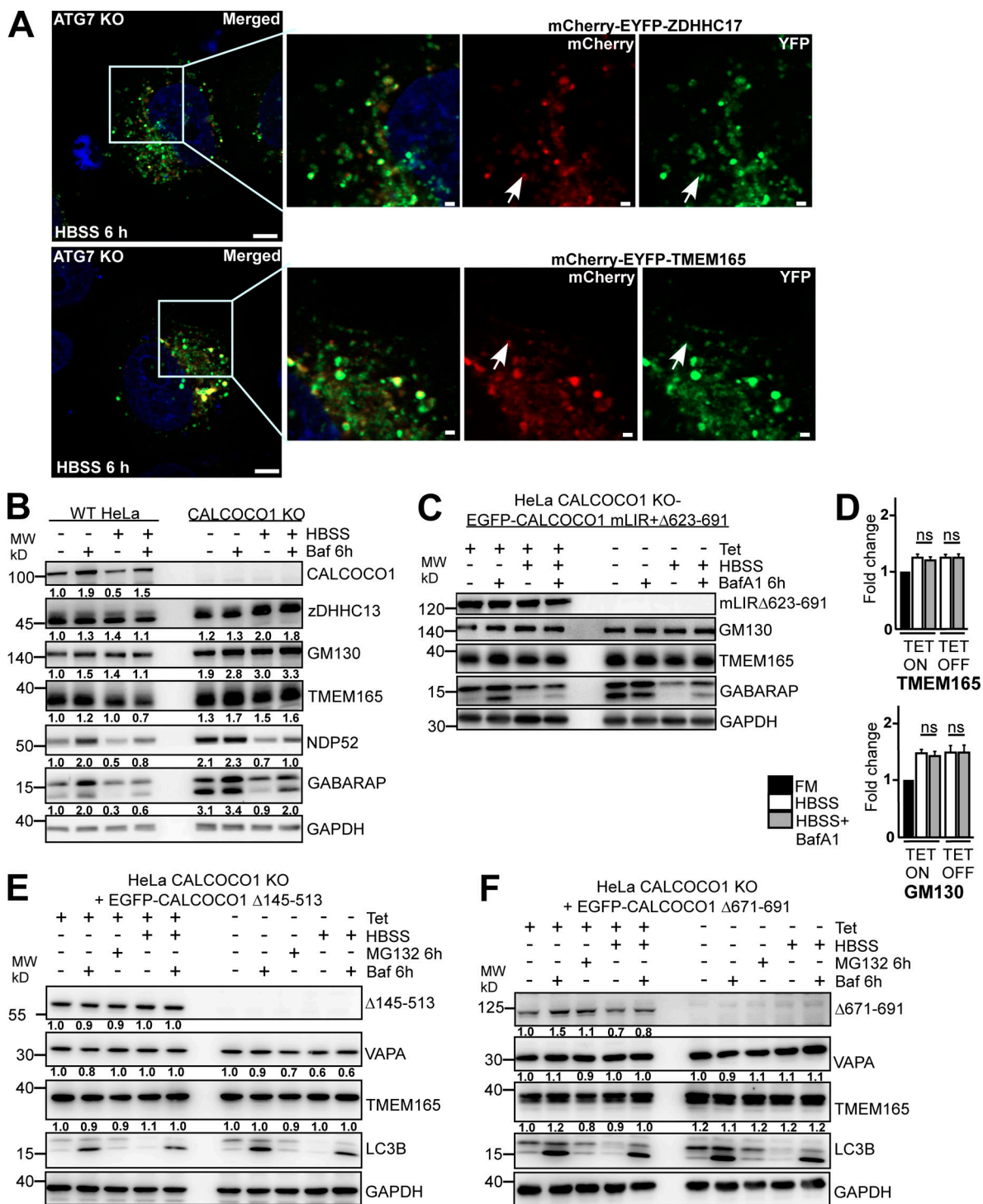
Figure S3. **CALCOCO1-dependent Golgiphagy is mediated by macroautophagy and depends on the ATG8 interaction motifs, but not the FFAT-like motif. (A)** ATG7 KO cells were transiently transfected with mCherry-EYFP-ZDHHC17 or mCherry-EYFP-TMEM165. 24 h after transfection, the cells were treated or not with HBSS as indicated. The arrow points to red-only puncta. Bars represent 5 μm (main) and 1 μm (insets). **(B)** Western blot analysis of HeLa WT or HeLa CALCOCO1 KO cells treated as indicated and analyzed by immunoblotting with the indicated antibodies. Numbers below the blots represent relative intensity of the bands in the blots shown, normalized against loading control. The panels are collected from more than one Western blot experiment, but only a single GAPDH loading control is shown. **(C and D)** HeLa-CALCOCO1 KO cells reconstituted with EGFP-CALCOCO1(mutLIR+Δ623–691) were left uninduced or were induced for 24 h and then either left untreated or treated as indicated. Cell lysates were analyzed by immunoblotting using the indicated antibodies. The error bars in D represent the mean ± SD of band intensities relative to the loading control from three independent experiments quantified using ImageJ. Statistical comparison was analyzed by one-way ANOVA followed by Tukey multiple comparison test. **(E and F)** HeLa-CALCOCO1 KO cells reconstituted with EGFP-CALCOCO1 Δ145–513 (E) or EGFP-CALCOCO1 Δ623–691 (F) were left uninduced or were induced for 24 h and then treated as indicated. Cell lysates were analyzed by immunoblotting using the indicated antibodies. Numbers below the blots represent relative intensity of the bands in the blots shown, normalized against loading control. MW, molecular weight.